Prediction of Wear Behavior in Surface Contact Using CDM and ANN Models

Sahar Ghatrehsamani [1,*], Mohammad Silani [2], Saleh Akbarzadeh [2], and Shirin Ghatrehsamani [2]

[1] Department of Mechanical Engineering, Isfahan University of Technology, Isfahan, Iran
[2] Department of Agricultural and Biological Engineering, Penn State University, University Park, USA
Email: s.ghatreh@alumni.iut.ac.ir (S.G.); silani@iut.ac.ir (M.S.); s.akbarzadeh@iut.ac.ir (S.A.); spg5994@psu.edu (Sh.G.)
*Corresponding author

***Abstract*—The objective of this study is to investigate and predict wear behavior in contacting surfaces through an integrated approach that combines Continuum Damage Mechanics (CDM) and Artificial Neural Networks (ANN). Pin on disk wear experiments were performed under dry conditions using three engineering materials ST37, C45E4, and Al7075 with variations in load, sliding speed, and hardness systematically designed using a full factorial Design of Experiments (DOE). The CDM model quantified material degradation and estimated wear coefficients, which were then used as training data for a feed-forward back-propagation ANN. Both models were validated against independent experimental data. Results indicate that the ANN model achieved high prediction accuracy (average error <5%), outperforming the CDM model (average error ≤12%). Scanning Electron Microscopy (SEM) revealed adhesive wear as dominant in the steels, while Al7075 exhibited reduced wear due to higher hardness. The interaction effects showed that load and sliding speed have significant influences on wear, whereas hardness plays a secondary role. The findings establish a robust framework for wear prediction, process optimization, and potential real-time monitoring in engineering applications, demonstrating the effective integration of physics-based and data-driven modeling in predictive tribology.**

***Keywords*—tribology, surface wear, Continuum Damage Mechanics (CDM), steady-state, Artificial Neural Network (ANN)**

I. Introduction

Tribology remains a vital field of study in modern engineering, influencing nearly every aspect of industrial and daily life. Among its fundamental phenomena, wear is a complex process involving the progressive removal or alteration of material from contacting surfaces due to mechanical interactions such as friction, adhesion, abrasion, erosion, or cyclic stresses. This phenomenon critically affects the performance, lifetime, and reliability of mechanical systems across diverse applications. Understanding wear mechanisms typically classified into adhesive, abrasive, and fatigue wear is essential for optimizing material selection, lubrication, and operating parameters to reduce energy consumption, minimize component failure, and enhance system durability. Despite decades of research, the integrative evaluation of classical mechanical models and Artificial Intelligence (AI)-based methods for wear prediction remains limited, particularly for specific material combinations and contact conditions [1].

Wear through fatigue mechanisms explains why harder materials may still experience wear when in contact with softer counterparts, indicating that adhesive wear encompasses both adhesion and fatigue processes [2]. Archard's [3] law provided the first quantitative framework for adhesive wear, relating wear volume to applied load, sliding distance, and material hardness. Continuum Damage Mechanics (CDM) further extended this understanding by offering a physics-based framework for quantifying material degradation, linking damage evolution to the reduction in elastic modulus and enabling the estimation of asperity strength and wear coefficients [4–20]. Notable works by Beheshti and Khonsari [13], Ghatrehsamani *et al.* [14–17, 19], and Salehi *et al.* [18, 20] applied CDM to predict wear behavior under varying loading, environmental, and contact conditions, including dry, lubricated, and so forth.

However, due to the limitations of purely mechanical approaches such as their dependence on simplifying assumptions and limited adaptability advanced AI techniques have been increasingly adopted to model complex tribological phenomena. Artificial Neural Networks (ANNs), in particular, have shown remarkable ability to learn nonlinear relationships from experimental data and deliver rapid, accurate predictions [21, 22]. Although ANN is considered a classical AI technique rather than an advanced one, it was selected in this study due to its proven reliability, interpretability, and suitability for comparison with the CDM model; moreover, its combination with other modeling approaches has continued to enhance prediction accuracy in various mechanical engineering applications. Early applications include studies by Jones *et al.* [23] on polymeric bearings, followed by Velten *et al.* [24], Palanisamy *et al.* [25],

Manuscript received September 5, 2025; revised October 14, 2025; accepted December 16, 2025; published March 13, 2026.

Bagga *et al.* [26], and others who successfully applied ANN to wear prediction in metals, wheels, and rails [27–31]. These efforts demonstrate the potential of AI-based approaches to complement or even surpass conventional predictive models, especially when large and high-quality experimental datasets are available.

To address the limitations of previous studies, this research develops and compares two predictive frameworks for wear: a physics-based CDM model and a data-driven ANN model. Pin-on-disk experiments are performed on three engineering materials ST37, C45E4, and Al7075 with different hardness levels and mechanical properties. Using a systematic factorial design, the study investigates the influence of load, sliding speed, and hardness on wear and validates model predictions against experimental data. The novelty of this study lies in integrating a physics-based CDM model with a data-driven ANN to predict wear behavior under various contacting surface conditions, bridging the gap between constitutive damage modeling and intelligent prediction techniques in tribological analysis.

The remainder of this paper is organized as follows: Section II introduces the modeling approaches, including the CDM and ANN formulations. Section III describes the experimental setup and methodology. Section IV presents the results, discussion, and analysis of wear mechanisms. Finally, Section V concludes the paper with key findings and implications for future work.

II. Modelling

In this research, the potential of the artificial neural network technique with the continuum damage mechanics method to analyze and predict the wear behavior of components during surface contact has been investigated.

A. Development of CDM Model

In this study, the baseline continuum damage mechanics model was extended through (i) material-specific calibration for C45E and Al7075, (ii) incorporation of heat treatment dependent mechanical properties, and (iii) coupling the CDM formulation with ANN for enhanced wear prediction. The integration of ANN with physics-based models, such as CDM, has been demonstrated to enhance predictive accuracy and generalization in wear analysis, as reported in previous studies [23–26, 28]. This study utilizes the damage definition introduced by Lemaitre [8]. The CDM model can accurately estimate the cycle count leading to failure, meaning crack initiation. When the damage parameter reaches its critical limit, crack initiation occurs, and the cycle ends. The critical damage parameter value for materials is obtained by tensile and fatigue testing [12]. Thus, the damage parameter is calculated per cycle from Eq. (1). The wear coefficient is determined by recording the number of cycles (j) completed until failure $W_k = 1/(3j)$.

$$D_{n,t} = 1 - \left(1 - D_{n,t-1}\right) \prod_{i=1}^{t} \frac{\left(\frac{1}{1+\frac{1}{R}}\Delta e_{i(t-1)}^{(H)} - \Delta e_{i(t)}^{(H)} g_{i(t)}\right) + \frac{3}{4}\frac{\sigma_f}{\left(2-\frac{1}{R}\right)C} - \frac{\Delta e_{i(t)}^{(H+C)}}{1+\frac{1}{R}} + \Delta e_{i(t)}^{(H)}\Delta e_{i(t)}}{\frac{1}{1+\frac{1}{R}}\Delta e_{i(t-1)}^{(H)} - \Delta e_{i(t)}^{(H)} g_{i(t)} + \frac{\sigma_f}{4\left(2-\frac{1}{R}\right)C} - \frac{\Delta e_{i(t)}^{(H+C)}}{1+\frac{1}{R}} + \Delta e_{i(t)}^{(H)}\Delta e_{i(t)}} \quad (1)$$

where C indicates the cyclic hardening modulus, R is the cyclic hardening exponent, S_f is the fatigue limit, and σ_f defines the true failure stress [13].

Eq. (1) is true if $\sigma_{max} \geq S_f$, otherwise $D_{AI_{(j)}} = D_{AI_{(j-1)}}$. $\Delta\varepsilon_{i(j)}$, $\Delta\varepsilon_{f(j)}$, $\Delta\varepsilon_{t(j)}$, and $\Delta\varepsilon_{t(j)}$ are initial, final plastic, threshold strain, and threshold plastic strain of damage growth in jth cycle, respectively and are obtained in terms of stress from Eqs. (2)–(4).

$$\Delta\varepsilon_{f(j)} = \left(\frac{\{(\sigma_{\max} - \sigma_{min})_{(j)}\}}{\left\{\left(2^{\left\{1-\frac{1}{R}\right\}}\right)C\left(1 - D_{AI(j-1)}\right)\right\}}\right)^{R} \quad (2)$$

$$\Delta\varepsilon_{i(j)} = \left(\frac{\sigma_{min(j)}}{\left\{\left(2^{\left\{1-\frac{1}{R}\right\}}\right)C\left(1 - D_{AI(j-1)}\right)\right\}}\right)^{R} \quad (3)$$

$$\Delta\varepsilon_{t(j)} = \left(\frac{\Delta\sigma_{i(j)}}{\left\{\left(2^{\left\{1-\frac{1}{R}\right\}}\right)C\left(1 - D_{AI(j-1)}\right)\right\}} + \frac{S_f}{\left\{\left(2^{\left\{1-\frac{1}{R}\right\}}\right)C\right\}}\right)^{R} \quad (4)$$

Under compressive loading and forward shear force, it can be suggested that cracks initiate and propagate through shear, leading to $\sigma_{max} = \mu_j f_p$ [16]. In the first cycle, σ_{min} is zero. The CDM model was computed using an in house MATLAB based finite element framework, chosen for its numerical efficiency, ease of implementing custom constitutive laws, and seamless integration with neural networks.

B. The Structure of the ANN Model

In this study, the feed-forward back-propagation neural network is utilized to predict component wear in systems experiencing relative motion. This neural network architecture comprises an input layer, one or more hidden layers where the relationships between inputs and outputs are modeled and encoded via the CDM model, and an output layer that generates the corresponding outputs (wear). The precision of the prediction relies heavily on the quality and effectiveness of the training process. The architecture of a feed-forward, three-layer back propagation neural network is depicted in Fig. 1.

In this study, the ANN was trained using data generated from the CDM model rather than employing a Physics Informed Neural Network (PINN). While PINNs inherently integrate governing equations into the learning process, their implementation typically demands extensive computational resources and complex equation handling. The proposed ANN-CDM hybrid model, however, offers a more practical framework that preserves the physical basis of the CDM model while leveraging the ANN's

capacity for nonlinear regression and generalization. This approach achieves high predictive accuracy with reduced computational cost and implementation complexity.

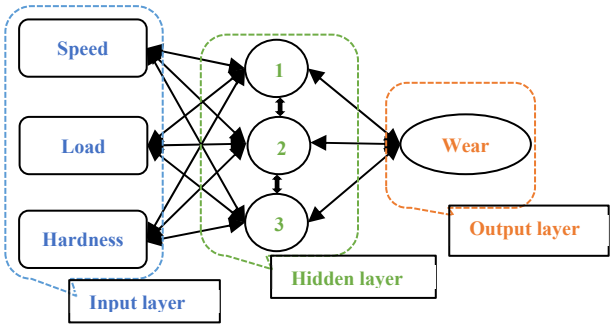

Fig. 1. The design of the artificial neural network model.

The configuration of the ANN is denoted as 3:3:1, indicating three neurons in the input layer, three in the hidden layer, and one in the output layer. The single neuron in the output layer represents the predicted component wear value. The inputs to the network speed, load, and hardness are used to evaluate component wear. The optimal number of neurons in the hidden layer, determined through experimentation with various configurations, was found to be three. It is worth noting that no definitive rule exists for selecting the number of hidden neurons. The learning process relies on the back propagation algorithm.

Error signals, generated from the difference between the calculated and actual outputs, are propagated backward from the output layer to preceding layers to adjust their weights. The hidden layer begins with a single neuron, and additional neurons are incrementally introduced. This process continues until no significant enhancement in the network's performance is observed. The network's accuracy is assessed using the mean squared error between observed and predicted values during training. When the average error falls below the predefined target threshold, the training process concludes, and the neural network is ready for validation.

III. Experimental Details

The laboratory tests have aimed to validate the wear predictions for realistic materials and then to train an artificial neural network.

TABLE I. Material Properties (From Experimental Measurements) [17]

Condition	Sample	E (GPa)	ρ (gr/mm^3)	S_f (GPa)	σ_f (GPa)	f_p (GPa)	R	C (GPa)	D_{cr}	h (GPa)
Simple	ST37	200	0.00785	0.20	0.37	0.25	~15	0.42	0.60	1.47
	C45E	210	0.00785	0.30	0.58	0.40	~18	0.65	0.42	1.96
	Al7075	72	0.00281	0.16	0.50	0.35	~10	0.30	0.30	1.60
Heat Treated	ST37	200	0.00785	0.24	0.42	0.20	~15	0.50	0.70	1.67
	C45E	210	0.00785	0.55	0.75	0.50	~20	1.00	0.60	2.50
	Al7075	72	0.00281	0.18	0.50	0.25	~8	0.20	0.20	1.77

A. Identification of Process Variables and Experimental Design

The tribological tests were carried out using a standard pin-on-disk configuration, in which the pin (made of bearing steel with a hardness of 220 HV) was stationary while the disk (specimens of ST37, C45E, and Al7075) rotated and served as the counter face material. The chemical compositions of the materials used in this study were taken according to ASTM standards. ST37 (ASTM A36 equivalent) is a mild structural steel containing approximately 0.17% C, 1.4% Mn, and small amounts of Si, P, and S. C45E (AISI 1045 equivalent) is a medium carbon steel with about 0.45% C and 0.75% Mn. Al7075 (ASTM B209) is an aluminum alloy consisting mainly of Al with alloying elements Zn (≈5.6%), Mg (≈2.5%), Cu (≈1.6%), and small additions of Cr and Fe. The disks are 5 mm thick and 50 mm in diameter, and the pins are cylindrical with a diameter of 17 mm. The material specifications of the work piece (disks) used in the experiment are detailed in Table I. ST37 is a low-carbon structural steel commonly used in manufacturing and construction due to its good weld ability and ductility. It serves as a baseline material with relatively low hardness. C45E4 is a medium-carbon steel with higher strength and hardness compared to ST37. Al7075 is a high-strength aluminum alloy known for its lightweight properties and excellent fatigue resistance, extensively used in aerospace and transportation industries. The selection aimed to cover a wide range of mechanical behaviors, from ductile low-hardness steel to high-strength aluminum, to test the robustness and generalizability of the predictive models. The samples to be hardened are placed inside the furnace and heated to a temperature of 250 °C. The samples are retained at this temperature for a period of two hours, after which they are rapidly cooled (water quenching). Light/low-temperature heat treatments (e.g., hardening up to ~250 °C or stress relief) usually do not significantly affect the Young's modulus, although hardness and tensile strength may increase.

Mechanical properties for C45E and Al7075 were experimentally determined through tensile and hardness tests (with the SANTAM STM-50 tensile testing machine (ASTM E8/E8M)), while CK45 properties were adopted from Ref. [17] for comparison. The hardness values included in the analysis represent the variations induced by the applied heat treatments and were incorporated as essential CDM model inputs to assess the model's robustness across materials with distinct hardening responses. Key process parameters influencing specimen wear, such as speed (S_V), load (F_L), and hardness (h), have been chosen as factors for performing the experiments and for developing CDM models. The tribological test

parameters were selected with reference to relevant industrial applications and existing literature, ensuring realistic wear conditions while maintaining test repeatability and avoiding thermal or mechanical distortions. To investigate the influence of these factors on wear behavior, a three-level, three-factor full factorial Design of Experiments (DOE) was implemented. This method was selected to allow systematic evaluation of all main effects and interactions among the variables. The test levels for each parameter are already embedded in the test matrix and summarized through experimental results in Table II. Hardness values were also varied through material selection and heat treatment (see Table I).

TABLE II. LEVELS OF TEST PARAMETERS USED IN THE FULL FACTORIAL DESIGN

Parameter	Symbol	Level 1	Level 2	Level 3
Sliding speed (m/s)	S_v	0.1	0.2	0.3
Normal Load (N)	F_L	10	20	30
Hardness (GPa)	h	~1.47	~1.96	~2.50

TABLE III. THE EXPERIMENTAL RESULTS

Experimental Sets	Exp. No	Speed (m/s)	Load (N)	Hardness (GPa)	Mean COF	Wear Volume (mm^3)
The first set of experimental	1	0.1	10	1.47	0.40	1.52
	2	0.1	10	1.96	0.39	1.43
	3	0.1	10	1.60	0.41	1.70
	4	0.1	20	1.47	0.43	2.75
	5	0.1	20	1.96	0.41	2.15
	6	0.1	20	1.60	0.45	3.30
	7	0.1	30	1.47	0.44	3.69
	8	0.1	30	1.96	0.43	3.25
	9	0.1	30	1.60	0.49	4.59
	10	0.2	10	1.47	0.45	2.00
	11	0.2	10	1.96	0.43	1.85
	12	0.2	10	1.60	0.50	2.31
	13	0.2	20	1.47	0.50	3.35
	14	0.2	20	1.96	0.49	3.12
	15	0.2	20	1.60	0.52	4.76
	16	0.2	30	1.47	0.50	6.87
	17	0.2	30	1.96	0.50	5.54
	18	0.2	30	1.60	0.55	7.33
	19	0.3	10	1.47	0.53	3.65
	20	0.3	10	1.96	0.51	3.41
	21	0.3	10	1.60	0.55	4.11
	22	0.3	20	1.47	0.53	5.34
	23	0.3	20	1.96	0.52	4.56
	24	0.3	20	1.60	0.56	5.98
	25	0.3	30	1.47	0.55	8.87
	26	0.3	30	1.96	0.54	7.94
	27	0.3	30	1.60	0.61	9.50
The second set of experimental	1	0.1	10	1.67	0.39	1.23
	2	0.1	10	2.50	0.36	1.13
	3	0.1	10	1.77	0.41	1.60
	4	0.1	20	1.67	0.41	2.18
	5	0.1	20	2.50	0.38	1.79
	6	0.1	20	1.77	0.45	2.84
	7	0.1	30	1.67	0.43	3.50
	8	0.1	30	2.50	0.39	3.15
	9	0.1	30	1.77	0.49	4.52
	10	0.2	10	1.67	0.45	1.42
	11	0.2	10	2.50	0.43	1.15
	12	0.2	10	1.77	0.50	1.95
	13	0.2	20	1.67	0.49	3.00
	14	0.2	20	2.50	0.44	2.84
	15	0.2	20	1.77	0.52	3.62
	16	0.2	30	1.67	0.49	6.00
	17	0.2	30	2.50	0.45	5.32
	18	0.2	30	1.77	0.55	6.50
	19	0.3	10	1.67	0.51	1.45
	20	0.3	10	2.50	0.48	2.00
	21	0.3	10	1.77	0.56	2.35
	22	0.3	20	1.67	0.52	4.23
	23	0.3	20	2.50	0.50	4.02
	24	0.3	20	1.77	0.60	4.75

Dry sliding wear tests (with Pin-on-Disc Wear Tester (ASTM G99)) have been conducted on these specimens at three different speeds (0.1, 0.2, and 0.3 m/s). Three distinct loads (10, 20, and 30 N) have been applied to specimens made of ST37, C45E, and Al7075 with varying hardness levels (before and after heat treatment at 250 °C). The sliding speeds and normal loads were selected to verify the stable and accurate operation of the pin-on-disk tribometer within its functional range. Hardness was considered as an input parameter, representing an intrinsic material property that influences wear behavior under identical test conditions. The three hardness values listed in Table II correspond to the materials ST37, C45E, and Al7075 alloy. The hardness values of the materials were measured using the Vickers microhardness test (HV) according to ASTM E384 standards. The obtained hardness values were converted into GPa for consistency with input parameters used in the numerical models. Each test was repeated at least three times to ensure the repeatability of the results, and the average of these repetitions was considered for each case and for training the artificial intelligence model. The output of the wear testing device, measured by its load cell, is an Excel file containing the coefficient of friction graph versus time or sliding distance. And then, the weight of the disk is recorded using a digital scale and using the density of steel, the mass reduction is converted into mm3. The wear of the counter face (pin) was not studied, as the focus of this research was on the wear performance of the disk specimens. The initial contact pressure for ST37, calculated based on Hertzian theory for a spherical pin with a radius of 17 mm and normal loads of 10–30 N, ranged approximately from 93–139 MPa.

The experimental data are divided into two separate sets. The first set is used alongside the CDM technique to extract data for training the artificial neural network. To validate and compare these models, their predicted results are evaluated against the second set of experimental results. Component wear is measured for each experiment by the difference in weight before and after the test. The measured values of wear for two groups of 27 experiments are presented in Table III. The end of each experiment and the distance taken to reach steady state have been considered (100 m). A fresh pin and disk are utilized for every trial and each test has been conducted a minimum of twice. The disk's weight is measured with a digital scale accurate to 0.0001 g, and the mass loss is converted to mm^3 using the steel's density.

B. Key Observations from the Experimental Results

Among the three materials, Al7075 showed significantly higher wear resistance compared to ST37 and C45E4, which is attributed to its superior hardness-to-weight ratio and microstructural stability. The wear rate of ST37 was the highest, indicating its limited resistance to surface degradation under sliding contact. The experimental results confirmed the sensitivity of wear behavior to both mechanical loading and material properties. The experimental dataset provided a robust basis for training and validating the ANN model, as well as for comparing it with the CDM model.

The materials investigated in this study were metallic specimens with varying hardness values but similar base composition. This design ensured that the effect of mechanical properties rather than compositional differences dominated the wear behavior. The ANN and CDM model captured how hardness, as a material-dependent property, influenced the damage evolution rate. Although the present model does not explicitly include metal type as an independent input, future studies will extend the database to include distinct metallic and mineral compositions, allowing the hybrid framework to predict wear across a broader range of materials. The experimental dataset provides a robust basis for training and validating the ANN model, as well as for comparison with the CDM model. Overall, the results highlight that wear is a multifactorial phenomenon, where both operational parameters and material properties must be considered to accurately predict surface degradation.

IV. Result and Discussion

In this section, the predicted outputs from both the CDM and ANN models are evaluated against experimental data using the validation set.

A. Model Validation

The predicted values of wear by the CDM model are given in Table I. As shown in the last column of Table IV, the error percentage of the CDM model is acceptable compared to the experimental results. Therefore, the output data of the CDM model has been used to train the ANN model. Respectively, the number of learning methods, algorithms, learning rule, number of learning patterns used, and number of epochs are supervised learning, back propagation, gradient descent rule, and number of learning patterns, 27 and 100.

After training is successfully completed, to assess the performance of the classification by the trained artificial neural network, a dataset that was not part of the training process is used (the second set of experiments). The predicted values of wear by the ANN and CDM models are given in Table V. Despite the relatively small dataset, each sample represent a complete solution of wear evolution. The values for speed, load, and hardness in this table correspond to those in rows 1–24 of Table I.

Results in Table V presents the predicted outputs from both the CDM and ANN models and experimental results in terms of percentage error, showcasing the models' predictive accuracy. For wear prediction, the CDM model yields an average error of less than 12%, whereas the ANN model exhibits significantly better accuracy with an average error below 5%. These findings suggest that the ANN model, when trained within the applicable range, offers more precise predictions of wear than the CDM-based model.

TABLE IV. THE FIRST SET OF EXPERIMENTAL RESULTS

The First Set of Experimental					Wear Volume (mm^3)		Error
Exp. No	Speed (m/s)	Load (N)	Hardness (GPa)	Mean COF	EXP	CDM	CDM and EXP
1	0.1	10	1.47	0.40	1.52	1.43	5.76
2	0.1	10	1.96	0.39	1.43	1.38	3.67
3	0.1	10	1.60	0.41	1.70	1.64	3.42
4	0.1	20	1.47	0.43	2.75	2.71	1.27
5	0.1	20	1.96	0.41	2.15	2.02	6.12
6	0.1	20	1.60	0.45	3.30	3.21	2.59
7	0.1	30	1.47	0.44	3.69	3.39	8.20
8	0.1	30	1.69	0.43	3.25	3.00	7.84
9	0.1	30	1.60	0.49	4.59	4.11	10.39
10	0.2	10	1.47	0.45	2.00	1.84	8.15
11	0.2	10	1.69	0.43	1.85	1.78	3.58
12	0.2	10	1.60	0.50	2.31	2.21	4.11
13	0.2	20	1.47	0.50	3.35	3.16	5.66
14	0.2	20	1.69	0.49	3.12	2.92	6.37
15	0.2	20	1.60	0.52	4.76	4.60	3.24
16	0.2	30	1.47	0.50	6.87	6.71	2.21
17	0.2	30	1.69	0.50	5.54	5.36	3.16
18	0.2	30	1.60	0.55	7.33	6.94	5.29
19	0.3	10	1.47	0.53	3.64	3.29	9.82
20	0.3	10	1.69	0.51	3.41	3.11	8.74
21	0.3	10	1.60	0.55	4.11	3.65	11.15
22	0.3	20	1.47	0.53	5.34	4.96	7.18
23	0.3	20	1.69	0.52	4.56	4.31	5.37
24	0.3	20	1.60	0.56	5.98	5.74	4.01
25	0.3	30	1.47	0.55	8.87	8.27	6.67
26	0.3	30	1.69	0.54	7.94	7.51	5.38
27	0.3	30	1.60	0.61	9.50	9.09	4.35

TABLE V. COMPARISON OF PREDICTED AND EXPERIMENTAL RESULTS

The Second Set of Experimental		Wear Volume (mm^3)			Error	
Exp. No	Mean COF	EXP	ANN	CDM	ANN and EXP	CDM and EXP
1	0.39	1.23	1.20	1.61	2.14	5.55
2	0.36	1.13	1.11	1.08	1.23	4.51
3	0.41	1.60	1.58	1.54	0.72	3.45
4	0.41	2.18	2.11	2.02	2.89	7.29
5	0.38	1.79	1.70	1.59	4.56	10.89
6	0.45	2.84	2.70	2.50	4.89	11.72
7	0.43	3.50	3.40	3.26	2.68	6.74
8	0.39	3.15	3.09	2.99	1.89	5.16
9	0.49	4.52	4.47	4.32	0.94	4.34
10	0.45	1.42	1.35	1.27	4.32	10.21
11	0.43	1.15	1.14	1.11	0.48	3.16
12	0.50	1.95	1.90	1.83	2.47	5.93
13	0.49	3.00	2.87	2.70	4.01	9.82
14	0.44	2.84	2.73	2.60	3.65	8.47
15	0.52	3.62	3.44	3.20	4.77	11.55
16	0.49	6.00	5.80	5.51	3.29	8.17
17	0.45	5.32	5.21	5.03	1.98	5.38
18	0.55	6.50	6.40	6.20	1.47	4.51
19	0.51	1.45	1.41	1.35	2.57	6.66
20	0.48	2.00	1.97	1.90	1.56	5.00
21	0.56	2.35	2.34	2.29	0.34	2.35
22	0.52	4.23	4.19	4.05	0.87	4.24
23	0.50	4.02	4.01	3.93	0.21	2.22
24	0.60	4.75	4.62	4.42	2.73	6.91
25	0.54	8.23	7.97	7.75	3.14	8.05
26	0.52	7.70	7.46	7.03	3.99	9.67
27	0.66	8.67	8.34	7.91	3.76	8.75

Although various machine learning algorithms could be applied, the ANN is selected due to its superior capability to capture nonlinear, multivariate relationships inherent in wear behavior. Comparative trials have shown that while a standalone ANN could approximate the experimental data, the CDM and ANN hybrid model achieved higher accuracy and generalization, demonstrating that integrating physical knowledge from CDM enhances the predictive performance of the neural network.

B. Wear Mechanisms Analysis Based on SEM

Fig. 2 shows Scanning Electron Microscopy (SEM) images of the worn surfaces (before heat treatment) of the ST37, C45E4, and Al7075 samples under load 10 N and speed 0.1 m/s at 50 μm magnification (ASTM E766).

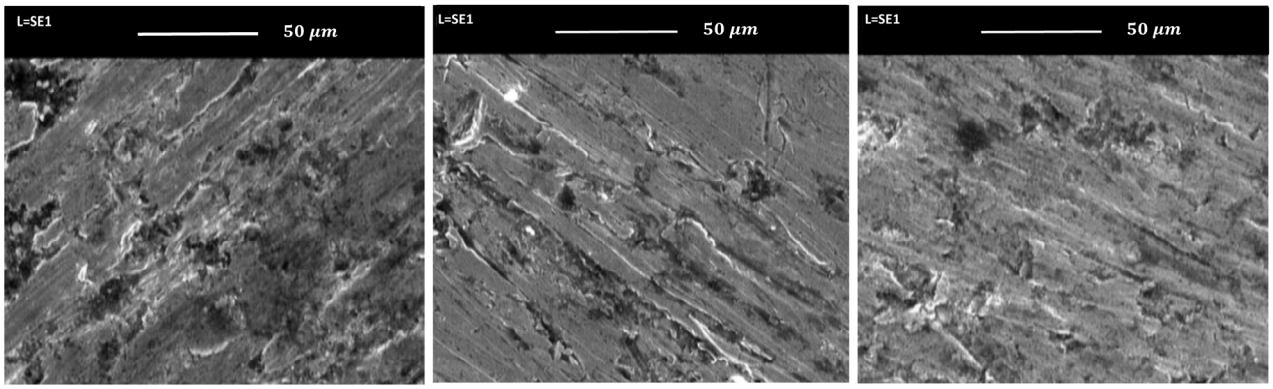

(a) (b) (c)

Fig. 2. SEM image of worn surfaces (before heat treatment): (a) ST37; (b) C45E4; and (c) Al7075 wear tests.

The images reveal that adhesive wear is the predominant mechanism, evidenced by micro-welding and material transfer in ST37 and C45E4 steels. Minor abrasive wear features are also present. The Al7075 alloy exhibits smaller, more uniform wear tracks with limited debris, likely due to its higher hardness and different surface energy, which reduce adhesion tendencies. The distinct wear behaviors across these materials justify their selection for this study, as they provided a diverse representation of tribological responses under similar contact conditions. This variety enhances the generalizability of the developed models.

C. Interaction Effect of Parameters on Wear

The interaction effects of speed, load, and hardness on wear volume were investigated using the predicted results from the ANN model. Fig. 3(a) and (b) present surface plots illustrating how combinations of these parameters influence wear behavior.

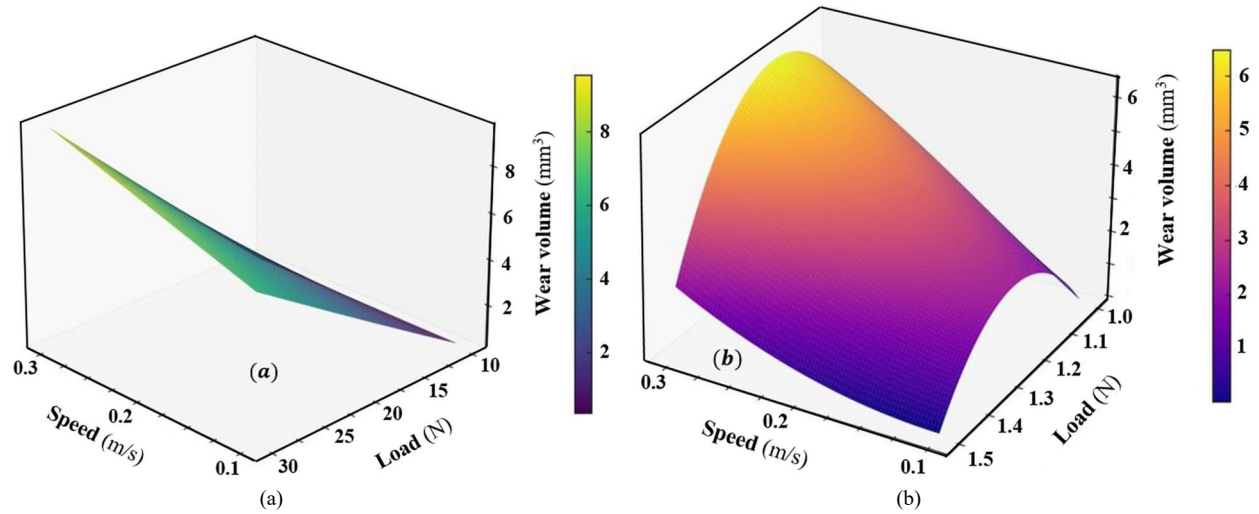

(a) (b)

Fig. 3. Surface plot for the interaction effect of (a) speed and load and; (b) speed and hardness on.

From Fig. 3(a), it is clear that wear volume increases significantly with both speed and load. The highest wear occurs at the maximum tested load of 30 N combined with the highest speed of 0.3 m/s, indicating that these conditions cause the most severe surface degradation. This trend is consistent with classical wear theory, where higher contact forces and increased sliding velocity typically accelerate wear processes. Fig. 3(b) shows the interaction effect of speed and hardness on wear. As expected, materials with higher hardness generally exhibit lower wear volumes under similar speed conditions. However, the surface plot reveals a nonlinear curvature in the variation of wear with both hardness and speed. This curvature suggests that: At lower to moderate speeds, increasing hardness effectively reduces wear, which aligns with expected behavior based on Archard's law and fundamental tribological principles. However, at higher sliding speeds, even hard materials show a noticeable increase in wear volume. This indicates that the beneficial effect of hardness diminishes as speed increases, possibly due to thermal softening, tribo-oxidation, or instabilities in surface microstructure that may arise during high-speed sliding. Conversely, materials with lower hardness are more susceptible to wear, especially at higher speeds, reinforcing the critical role of hardness for durability at moderate conditions. These observations highlight the complex and nonlinear interaction between material hardness and operational speed. Increasing hardness alone may not be sufficient to counteract the accelerated wear caused by higher sliding velocities. Therefore, careful

selection and optimization of both material properties and process parameters are essential to minimize wear under demanding conditions. The findings also provide valuable insight for process design and material selection in applications involving surface contact and friction. To further validate the curvature trend observed in Fig. 3(b), future studies may focus on detailed wear mechanism analysis through surface characterization techniques such as SEM imaging or profilometry at critical combinations of speed and hardness.

D. Interaction Effect Analysis Using ANOVA

To quantitatively evaluate the influence of speed, load, and hardness on wear volume, as well as their interaction effects, an Analysis of Variance (ANOVA) was conducted using the experimental data. Table VI summarizes the ANOVA results, including main parameters and their interactions.

In this analysis, the *p*-value represents the probability that the observed effect is due to chance, with values less than 0.05 indicating statistical significance at the 95% confidence level. The F-value indicates the ratio of variance explained by the factor to the unexplained variance, showing the significance of each parameter or interaction. The results reveal that load has the most significant effect on wear volume, followed by speed. Both parameters have *p*-values far below 0.05, confirming their strong impact. Hardness shows some influence but is not statistically significant at the 5% confidence level in the tested conditions. Importantly, the interaction between speed and load is significant, indicating a combined effect on wear volume and friction behavior. Other interaction terms, such as speed × hardness and load × hardness, were not statistically significant. These findings are consistent with the experimental observations and the 3D interaction plots, confirming that wear behavior is strongly affected by the combined effects of speed and load, while hardness plays a relatively minor role. Although the ANOVA analysis indicated that the applied load has the highest F-value (71), confirming its dominant effect on wear, the results also showed that speed and hardness play secondary but meaningful roles. The CDM and ANN hybrid model revealed that hardness influences the damage accumulation rate by modifying the contact stress and plastic deformation behavior. Therefore, despite its lower statistical contribution compared to load, hardness remains an essential input parameter to reflect the material's resistance to surface damage and wear evolution.

TABLE. VI. COMPARISON OF PREDICTED AND EXPERIMENTAL RESULTS

Significance	*p*-value	F-value	Parameter
Highly significant	0.0000123	20.98	Speed
Highly significant	0.00000000079	71.31	Load
Not significant at 5% level	0.0845	2.80	Hardness
Significant	0.0041	9.25	Speed × Load
Not significant	0.29	1.15	Speed × Hardness
Not significant	0.51	2.03	Load × Hardness

V. CONCLUSION

This study developed and compared two complementary approaches for predicting wear behavior in contacting surfaces: a physics-based CDM model and a data-driven ANN model. Experimental investigations were carried out on three engineering materials ST37, C45E4, and Al7075 under varying loads, sliding speeds, and hardness levels using a full factorial DOE. The CDM model provided a mechanistic understanding of material degradation and damage evolution, while the ANN model demonstrated superior predictive capability, achieving an average error below 5%, compared with ≤12% for the CDM model. SEM revealed adhesive wear as the dominant mechanism in steels, whereas the aluminum alloy exhibited lower wear resistance due to its higher hardness and distinct microstructural behavior. The comparative analysis confirmed that combining CDM and ANN offers a robust and efficient framework for wear prediction, bridging the gap between physics-based modeling and data-driven learning. The findings underscore the potential of hybrid modeling in optimizing tribological performance, reducing experimental effort, and improving predictive accuracy for engineering applications.

Future research should focus on advancing the hybrid CDM and ANN framework by incorporating larger and more diverse datasets covering a wider range of materials and operating conditions. The integration of PINNs and uncertainty quantification is recommended to enhance model robustness, interpretability, and predictive confidence. Furthermore, multi-scale modeling approaches linking microstructural mechanisms to macroscopic wear responses should be developed to provide a more comprehensive understanding of wear behavior. Expanding the experimental database to include different metals, alloys, and composite materials will enable broader validation and generalization of the proposed model. Lastly, future efforts could explore real-time wear monitoring and predictive maintenance systems based on the proposed hybrid methodology for industrial implementation.

NOMINAL SYSTEM

C: Cyclic hardening modulus (Pa).
d: Sliding distance (m).
D_{AI}: Damage parameter.
E: Modulus of elasticity (undamaged) (Pa).
E_d: Modulus of elasticity (damaged) (Pa).
F_L: Applied load to the surface (N).
f_p: Material flow pressure (Pa).
h: Hardness.
j: Number of cycles.
R: Cyclic hardening exponent.

S_f: Fatigue limit (Pa).
S_v: Sliding speed (m/s).
V_{AI}: Wear volume (m3).
W_K: Wear coefficient.
$\Delta\varepsilon_i$: Initial strain in j^{th} cycle.
$\Delta\varepsilon_f$: Final plastic strain in j^{th} cycle.
$\Delta\varepsilon_t$: Threshold strain of damage growth in j^{th} cycle.
$\Delta\varepsilon_p$: Threshold plastic strain of damage growth in j^{th} cycle.
μ: Friction coefficient.
σ_f: Failure stress (Pa).
σ_{max}: Maximum normal stress (Pa).
σ_{min}: Minimum normal stress (Pa).

CONFLICT OF INTEREST

The authors declare no conflict of interest.

AUTHOR CONTRIBUTIONS

SG conducted the research and experiments, analyzed the data, and wrote the manuscript; MS designed the methodology and supervised the project; SA and ShG supervised the project as the advisor; all authors had approved the final version.

FUNDING

This work is based upon research funded by the Iran National Science Foundation (INSF) under project No. 4026797.

REFERENCES

[1] M. M. Khonsari, S. Ghatrehsamani, and S. Akbarzadeh, "On the running-in nature of metallic tribo-components: A review," *Wear,* vol. 474, 203871, 2021. https://doi.org/10.1016/j.wear.2021.203871
[2] A. Rosenfield, "Wear and fracture mechanics," *Fundamentals of Friction and Wear of Materials,* pp. 221–234, 1980. https://doi.org/10.1016/0956-716X(90)90117-Y
[3] J. Archard, "Contact and rubbing of flat surfaces," *Journal of applied physics,* vol. 24, pp. 981–988, 1953. https://doi.org/10.1063/1.1721448
[4] I. V. Kragelskii, *Friction and Wear,* 6th ed. London: Butterworths, 1965.
[5] B. Bhattacharya and B. Ellingwood, "Continuum damage mechanics analysis of fatigue crack initiation," *International Journal of Fatigue,* vol. 20, pp. 631–639, 1998. https://doi.org/10.1016/S0142-1123(98)00032-2
[6] B. Bhattacharya and B. Ellingwood, "A new CDM-based approach to structural deterioration," *International Journal of Solids and Structures*, vol. 36, pp. 1757–1779, 1999. https://doi.org/10.1016/S0020-7683(98)00057-2
[7] B. Bhattacharya, "A damage mechanics based approach to structural deterioration and reliability," Ph.D. dissertation, The Johns Hopkins Univ., 1997.
[8] J. Lemaitre, "A continuous damage mechanics model for ductile fracture," *Journal of Engineering Materials and Technology*, vol. 107, no. 1, pp. 83–89, 1985. https://doi.org/10.1115/1.3225775
[9] D. Krajcinovic, "Continuous damage mechanics revisited: Basic concepts and definitions," *Journal of Applied Mechanics*, vol. 52, no. 4, pp. 829–834, 1985. https://doi.org/10.1115/1.3169154
[10] M. Bryant, M. Khonsari, and F. Ling, "On the thermodynamics of degradation," in *Proc. the Royal Society A: Mathematical, Physical and Engineering Sciences*, 2008, vol. 464, pp. 2001–2014. https://doi.org/10.1098/rspa.2007.0371
[11] J. L. R. Desmorat and J. Lemaitre, *Engineering Damage Mechanics*, 1st ed. Springer-Verlag Berlin Heidelberg, 2005.
[12] S. Ghatrehsamani and S. Akbarzadeh, "Predicting the wear coefficient and friction coefficient in dry point contact using continuum damage mechanics," in *Proc. the Institution of Mechanical Engineers, Part J: Journal of Engineering Tribology*, 2019, vol. 233, pp. 447–455, https://doi.org/10.1177/1350650118785045
[13] A. Beheshti and M. M. Khonsari, "A thermodynamic approach for prediction of wear coefficient under unlubricated sliding condition," *Tribology Letters,* vol. 38, pp. 347–354, 2010. https://doi.org/10.1007/s11249-010-9614-4
[14] S. Ghatrehsamani, S. Akbarzadeh, and M. M. Khonsari, "Application of continuum damage mechanics to predict wear in systems subjected to variable loading," *Tribology Letters,* vol. 69, 163, 2021. https://doi.org/10.1007/s11249-021-01539-2
[15] S. Ghatrehsamani, S. Akbarzadeh, and M. M. Khonsari, "Experimental and numerical study of the running-in wear coefficient during dry sliding contact," *Surface Topography: Metrology and Properties,* vol. 9, 015009, 2021. doi: 10.1088/2051-672X/abbd7a
[16] S. Ghatrehsamani, S. Akbarzadeh, and M. M. Khonsari, "Experimentally verified prediction of friction coefficient and wear rate during running-in dry contact," *Tribology International,* vol. 170, 107508, 2022. https://doi.org/10.1016/j.triboint.2022.107508
[17] S. Ghatrehsamani, M. Silani, S. Akbarzadeh *et al.,* "Application of continuum damage mechanics for prediction of wear in tillage tools," *Smart Agricultural Technology,* vol. 10, 100852, 2025. https://doi.org/10.1016/j.atech.2025.100852
[18] S. Salehi, S. Ghatrehsamani, S. Akbarzadeh *et al.,* "Application of Continuum damage mechanics for prediction of wear with provision for sequential speed operation," *Tribology Letters,* vol. 70, 105, 2022. https://doi.org/10.1007/s11249-022-01645-9
[19] S. Ghatrehsamani, S. Salehi, S. Akbarzadeh *et al.,* "On the wear of coated surfaces under variable speed," *Tribology International,* vol. 187, 108677, 2023. https://doi.org/10.1016/j.triboint.2023.108677
[20] S. Salehi, S. Ghatrehsamani, S. Akbarzadeh *et al.,* "Prediction of wear in start-stop systems using continuum damage mechanics" *Tribology Letter*s, vol. 73, no. 1, 11. 2024. https://doi.org/10.1007/s11249-024-01943-4
[21] M. Marian and S. Tremmel, "Current trends and applications of machine learning in tribology—A review," *Lubricants,* vol. 9, 86, 2021. https://doi.org/10.3390/lubricants9090086
[22] A. Rosenkranz, M. Marian, F. J. Profito *et al.,* "The use of artificial intelligence in tribology—A perspective," *Lubricants,* vol. 9, 2, 2021. https://doi.org/10.3390/lubricants9010002
[23] S. P. Jones, R. Jansen, and R. L. Fusaro, "Preliminary investigation of neural network techniques to predict tribological properties," *Tribology Transactions,* vol. 40, pp. 312–320, 1997. https://doi.org/10.1080/10402009708983660
[24] K. Velten, R. Reinicke, and K. Friedrich, "Wear volume prediction with artificial neural networks," *Tribology International,* vol. 33, pp. 731–736, 2000. https://doi.org/10.1016/S0301-679X(00)00115-8
[25] P. Palanisamy, I. Rajendran, and S. Shanmugasundaram, "Prediction of tool wear using regression and ANN models in end-milling operation," *The International Journal of Advanced Manufacturing Technology,* vol. 37, pp. 29–41, 2008. https://doi.org/10.1007/s00170-007-0948-5
[26] P. Bagga, M. Makhesana, H. Patel *et al.,* "Indirect method of tool wear measurement and prediction using ANN network in machining process," *Materials Today: Proceedings,* vol. 44, pp. 1549–1554, 2021. https://doi.org/10.1016/j.matpr.2020.11.770
[27] T. Kolodziejczyk, R. Toscano, S. Fouvry *et al.,* "Artificial intelligence as efficient technique for ball bearing fretting wear damage prediction," *Wear,* vol. 268, pp. 309–315, 2010. https://doi.org/10.1016/j.wear.2009.08.016
[28] A. Shebani and S. Iwnicki, "Prediction of wheel and rail wear under different contact conditions using artificial neural networks," *Wear,* vol. 406, pp. 173–184, 2018. https://doi.org/10.1016/j.wear.2018.01.007
[29] F. Alambeigi, S. M. Khadem, H. Khorsand *et al.* "A comparison of performance of artificial intelligence methods in prediction of dry sliding wear behavior," *The International Journal of Advanced Manufacturing Technology,* vol. 84, pp. 1981–1994, 2016. https://doi.org/10.1007/s00170-015-7812-9

[30] A. Bustillo, D. Y. Pimenov, M. Matuszewski *et al.* "Using artificial intelligence models for the prediction of surface wear based on surface isotropy levels," *Robotics and Computer-Integrated Manufacturing,* vol. 53, pp. 215–227, 2018. https://doi.org/10.1016/j.rcim.2018.03.011

[31] P. M. Sieberg, D. Kurtulan, and S. Hanke, "Wear mechanism classification using artificial intelligence," *Materials,* vol. 15, 2358, 2022. https://doi.org/10.3390/ma15072358